Monodispersing Eu^{3+} and Li^{+} codoped CaF_2 nanoparticles for efficient luminescence

Ting Fan[1], Jiantao Lü[2] ✉, Yongfa Huang[1], Guoji Li[1]

[1]*School of Materials Science and Energy Engineering, Foshan University, Foshan 528000, People's Republic of China*
[2]*School of Physics and Optoelectronic Engineering, Foshan University, Foshan 528000, People's Republic of China*
✉ *E-mail: keentle@gmail.com*

Published in Micro & Nano Letters; Received on 25th September 2017; Revised on 7th November 2017; Accepted on 23rd November 2017

Monodisperse oleic acid (OA) modified Eu^{3+} and Li^{+} codoped CaF_2 nanoparticles are presented in this work. The as-obtained nanoparticles, with a hexagonal shape, can be well-dispersed in organic apolar solvents. The incorporation of Li^{+} ions in CaF_2:Eu^{3+} does not lead to new crystalline phases. The main diffraction peaks are found to shift to small angles when codoped with 7 mol% Li^{+}, while a reverse shift can be noted with the codoping amount increasing to 9 mol% Li^{+}, indicating that the codoped Li^{+} enables the crystal field environment of Eu^{3+} to be changed. The excitation and luminescence intensities of all peaks indexed to Eu^{3+} have enhanced apparently when codoped with 7 mol% Li^{+} ions. The lifetime of the $^5D_0$ state of Eu^{3+} ions is also increased by introducing 7 mol% of Li^{+} ions.

1. Introduction: Over nearly two decades, lanthanide ion-doped nanomaterials have attracted great scientific interest. Luminescent nanomaterials exhibit the potential for significant applications like medical and biological labels [1], displays [2], solar cells [3] and catalysts [4]. Calcium fluoride (CaF_2) can serve as an excellent host because of its high transparency over the vacuum ultraviolet (~200nm) to infrared (IR; ~10 μm) range, in addition to its low phonon energy (~323 cm^{-1}) [5], revealing low rates of non-radiative relaxations. All Ca^{2+} precursors are low-effective and easy to obtain. Furthermore, the ionic radius of Ca^{2+} is close to that of lanthanide dopant ions, which indicates that crystal defects and lattice stress can be reduced when Ca^{2+} ions are replaced by lanthanide ions [6]. From biological applications, it is worth noting that CaF_2 is a very interesting host because calcium is a non-toxic element [1].

Recently, to improve the luminescence of lanthanide ions using various methods has gathered increasing attention [7–9]. The enhancement of Ln^{3+} emission is very important because the amount of Ln^{3+} can be decreased and results in the reduction of the toxicity of Ln^{3+} for biological applications. The luminescence enhancement through Ln^{3+} doping is also useful for optoelectronic device applications. Recently, Yin *et al.* found that the alkali ion codoping approach could enhance the up conversion luminescence intensity of CaF_2:Yb^{3+}, Er^{3+} nanoparticles efficiently [10]. Singh *et al.* found a luminescence enhancement for CaF_2:Eu^{3+} nanoparticles upon codoping of Mn^{2+}[11]. However, the luminescence improvement of monodisperse oil-soluble Eu^{3+}-doped CaF_2 nanoparticles by Li^{+} codoping has rarely been reported. Oil-soluble Eu^{3+}-doped CaF_2 nanoparticles can be changed into water-soluble nanoparticles for biological applications by simple chemical reactions. In this Letter, we show the synthesis and optical properties of Li^{+} codoped oleic acid (OA)-modified CaF_2:Eu^{3+} nanoparticles. Among Ln^{3+} ions, Eu^{3+} ions are chosen for the doping because of a good source of the red emitter. The luminescence intensity of all peaks related to Eu^{3+} can be enhanced apparently when codoped with 7 mol% Li^{+} ions. Therefore, this study provides insight into how to easily improve the emission intensity of Ln^{3+} ion-doped fluoride nanoparticles.

2. Experimental

2.1. Materials: $CaCl_2$ (96%), Eu_2O_3 (99.9%), $LiNO_3$ (99.9%), NaOH (97%), NH_4F (98%), HNO_3 (65%), OA (85%) and ethanol (99.7%) were purchased from Aladdin Reagent Company. All of the chemical reagents used in this experiment were of analytical grade without further purification. Deionised water was used throughout the experiment. $Eu(NO_3)_3$(0.05M) solution was prepared by dissolving proper amount of Eu_2O_3 in HNO_3 at elevated temperature.

2.2. Synthesis of OA-modified CaF_2: Eu^{3+}, Li^{+} nanoparticles: In a typical process, 5 mol% Eu^{3+} doped CaF_2 nanoparticles were synthesised as follows. 3 ml of OA, 10 ml of ethanol and 0.08 g of NaOH were mixed together. Then the mixture was agitated to form a homogeneous transparent solution. Then 2.4 ml of $CaCl_2$ (0.4 M) aqueous solution and 1 ml of $Eu(NO_3)_3$ (0.05 M) aqueous solution were added to the mixture in order under vigorous stirring to form a homogeneous milky white solution. After that 4 ml NH_4F (1 M) aqueous solution was added into the mixture. The obtained mixture was stirred for 1 h and then transferred into a 50 ml autoclave, sealed and treated with 160°C for 10 h. When the mixture was cooled to room temperature, the resulting solutions were centrifuged for 10 min at 5000 rpm to obtain the powder products. The as-obtained powders were washed several times with ethanol to remove the excess OA, sodium oleate, and other remnant impurities. The resulting nanoparticles were dried in air at 60°C for 12 h. The addition of 7 and 9 mol% Li^{+} into CaF_2:Eu^{3+} nanoparticles were synthesised in a similar process by adding 1.4 and 1.8 ml of $LiNO_3$ (0.05 M) aqueous solution before the introduction of the NH_4F solution.

2.3. Characterisation: Powder X-ray diffraction (XRD) measurements were obtained by a Bruker D8 Advance X-ray diffractometer with Cu Kα radiation ($\gamma = 0.15406$ nm). Transmission electron microscopy (TEM), high-resolution transmission electron microscopy (HRTEM) images and selected area electron diffraction patterns (SAED) were obtained by using an FEI Tecnai G20 transmission electron microscope at an acceleration voltage of 200 kV. The Fourier transform infrared (FT-IR) spectra were obtained by using a Magna-IR 750 Fourier transform infrared spectrometer. Excitation and photoluminescence spectra were measured by using a Hitachi F-4600 spectrofluorometer. The luminescence delay profiles were measured by using a Jobin-Yvon Triax320 spectrometer. All measurements were performed at room temperature and under the same environmental conditions.

3. Results and discussions

3.1. Structure and morphology of the as-prepared nanoparticles: Fig. 1*a* shows the XRD patterns of CaF_2:Eu^{3+} nanoparticles codoped with 0, 7 and 9 mol% Li^{+} ions. All diffraction peaks of

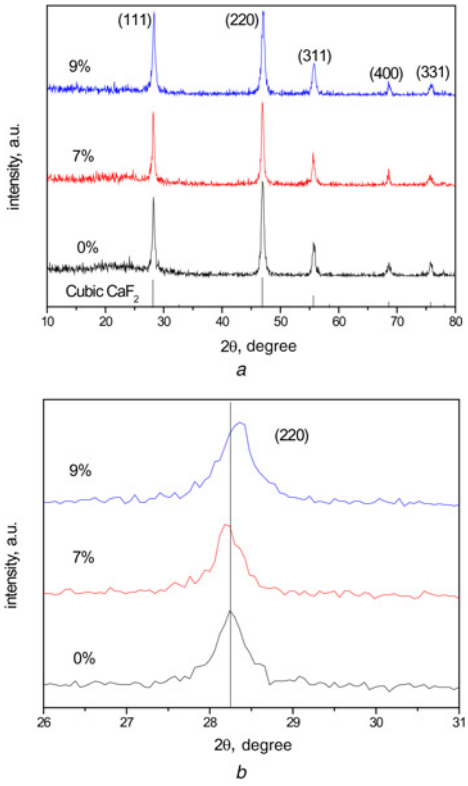

Fig. 1 *XRD patterns of the samples*
a XRD pattern of CaF_2:Eu^{3+} nanoparticles codoped with 0, 7 and 9 mol% Li^+ ions
b Magnified XRD pattern of the main peak for the two samples

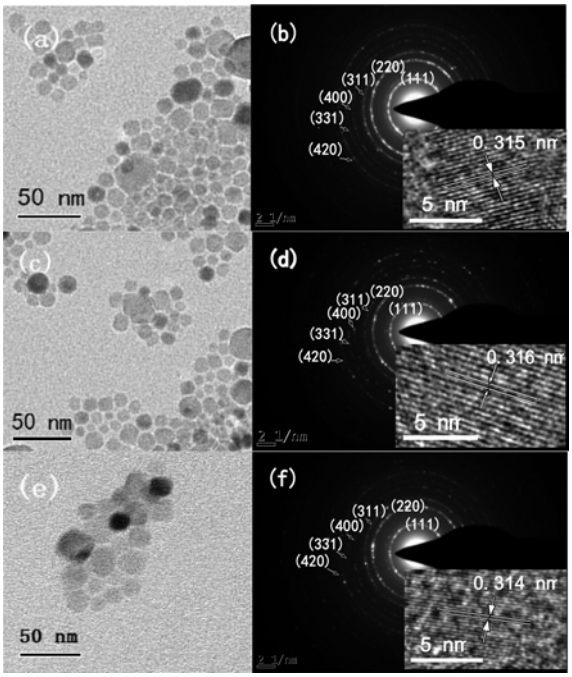

Fig. 2 *Morphology of nanoparticles*
a TEM image of CaF_2:Eu^{3+}
b SAED and inserted HRTEM image of CaF_2:Eu^{3+}
c TEM image of CaF_2:Eu^{3+} codoped with 7 mol% Li^+
d SAED and inserted HRTEM image of CaF_2:Eu^{3+} codoped with 7 mol% Li^+
e TEM image of CaF_2:Eu^{3+} codoped with 9 mol% Li^+
f SAED and inserted HRTEM image of CaF_2:Eu^{3+} codoped with 9 mol% Li^+

the three samples could be indexed to the cubic structure pure phase of CaF_2, which was agreed with Powder Diffraction File PDF 35–0816. Codoping with Eu^{3+} and Li^+ ions did not introduce impurity peaks.

As shown in Fig. 1*b*, the diffraction peaks assigned to the (111) plane were found to shift slightly when codoped with Li^+. The 2θ values of 0, 7 and 9 mol% Li^+ ion codoped CaF_2:Eu^{3+} were measured to be 28.24° and 28.18°, 28.36° respectively. The *d*-spacing values belonging to the (111) plane of the three samples were calculated to be 3.157, 3.164 and 3.144 Å, respectively, according to the relation $2d_{(111)} \sin\theta = \lambda$, and then $d_{(111)} = (1.5405\ \text{Å}/2\sin\theta)$ [11]. The *d*-spacing values increased when codoped with 7 mol% Li^+ and reversed for codoping with 9 mol% Li^+. The ionic radius of Ca^{2+} and Li^+ is 1 and 0.76 Å, respectively. Li^+ ions could join the crystal site of Ca^{2+} easily through the replacement or occupation interstitial point of Ca^{2+}. Replacement with smaller ions could shrink the host lattice, whereas occupying interstitial points could expand the lattice. A small amount of Li^+ tend to replace Ca^{2+} and then started to occupy the interstitial site when codoping Li^+ up to 7 mol%. Excess Li^+ (9 mol%) squeezed lattice which could decrease the lattice constant. The tiny alteration of the *d*-spacing value meant that the codoping of Li^+ distorted the crystal structure slightly. The substitution and occupation interstitial site of Ca^{2+} ions could both tailor the local crystal field and influence the luminescence of Eu^{3+} [12].

The morphology of nanoparticles could be seen in Fig. 2. The TEM image shown in Fig. 2*a* indicated that the as-obtained CaF_2:Eu^{3+} nanoparticles were well-dispersed and had a hexagonal shape with a mean diameter of about 22 nm. The SAED pattern shown in Fig. 2*b* was consistent with a cubic structure of CaF_2, which showed two strong ring patterns ascribed to (111) and (220) planes and in good agreement with the XRD result. The inter-planar spacing of CaF_2:Eu^{3+} nanoparticles was about 0.315 nm, which was identical to the (111) facet distance of the bulk CaF_2 phase [13]. The morphology of 7 mol% Li^+ codoped CaF_2:Eu^{3+} nanoparticles are shown in Figs. 2*c* and *d*. When codoped with 7 mol% Li^+, there was little change in morphology with a slightly bigger mean diameter of about 24 nm and a slightly larger inter-planar spacing corresponding to the (111) plane of about 0.316 nm, which were in good agreement with the XRD results. The morphology of 9 mol% Li^+ codoped CaF_2:Eu^{3+} nanoparticles could be seen in Figs. 2*e* and *f*, which shows the similar morphology with a mean diameter of about 22 nm and inter-planar spacing corresponding to the (111) plane of about 0.314 nm, which was in agreement with the XRD results.

The FT-IR spectrum is shown in Fig. 3. Compared with [13], a similar FT-IR spectrum was obtained revealing the OA coating of the Li^+ non-codoped and codoped with 7 and 9 mol% CaF_2:Eu^{3+} nanoparticles. The broad absorption band occurring around 3436 cm^{-1} is characteristic of O–H stretching from OA and water molecules. The strong absorptions at 2923 and 2858 cm^{-1} are attributed to the asymmetric and symmetric C–H stretches, respectively. The peak at 3010 cm^{-1} indicates that the =C–H stretching vibration is involved. The absorption band at 2360 cm^{-1} is from KBr pellets used for recording the FT-IR spectrum. In the finger print region (below 1300 cm^{-1}), the absorption at 728 cm^{-1} proves the existence of the $(CH_2)_n$ $(n \geq 4)$ alkyl chains. In addition, the typical asymmetric and symmetric vibration of $-COO^-$ group peaks was detected about 1454 and 1565 cm^{-1}, which reveals the presence of carboxylate anions from the OA. The results from the spectrum suggested that codoping of Li^+ almost did not change the vibration band and thereby the multiphonon non-radiative rate which can influence the luminescence of Eu^{3+}.

The OA molecules with a long alkyl chain are present to control the growth of the nanocrystalline particles and to make the particles soluble in non-polar organic solution. The reaction process was similar to that reported by Zhang [13]. During the typical synthetic

doi: 10.1049/mnl.2017.0662

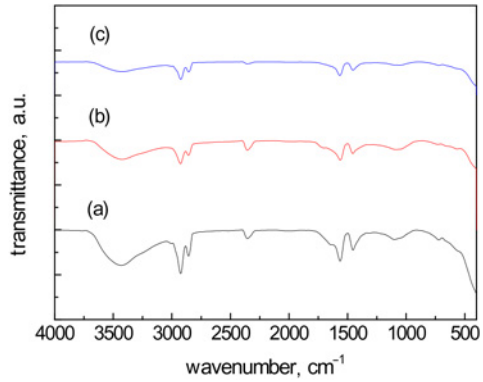

Fig. 3 *FTIR transmission spectra of CaF_2:Eu^{3+} nanoparticles*
a uncodoped with Li^+ ions
b codoped with 7 mol% Li^+ ions
c codoped with 9 mol% Li^+ ions

process, NaOH, OA, and ethanol were mixed firstly to form sodium oleate. The aqueous solution containing Ca^{2+} and Eu^{3+} was added drop wise to the sodium oleate solution containing excess ethanol and OA. Since a large amount of OA molecules existed in the system, the metal ions started to form complexes easily with OA molecules. Subsequently, the OA-capped metal ions reacted with F^- quickly to form the crystalline nuclei. The nuclei grew gradually in the solvothermal environment. Finally, the growth of the as-obtained nanocrystals was terminated by the OA molecules absorbed at the surface.

3.2. Photoluminescence properties of the nanoparticles: Fig. 4*a* shows the excitation (λ_{em} = 591 nm) spectra of CaF_2:Eu^{3+} nanoparticles codoped with 0, 7 and 9 mol% Li^+ ions. We focused on the range of excitation spectra in the 4f–4f transition of Eu^{3+}. The peaks were observed at 361, 375 and 394 nm correspond to $^7F_{0,1}\rightarrow{}^5D_0$, $^7F_{0,1}\rightarrow{}^5G_1$ and $^7F_0\rightarrow{}^5L_6$ transitions of Eu^{3+}, respectively. We could see from the excitation spectra that the intensity of all excitation peaks increased by about 1.8 times for 7 mol% Li^+ ions and decreased for 9 mol% Li^+. The enhancement of excitation intensity meant that the forbidden-transitions of Eu^{3+} ions were adjusted [14].

Fig. 4*b* shows the emission spectra of CaF_2:Eu^{3+} nanoparticles with 0, 7 and 9 mol% Li^+ under excitation through the direct f–f transition of the Eu^{3+} ion at 394 nm. The observed luminescence peaks at 591 and 612 nm were related to the $^5D_0\rightarrow{}^7F_1$ (magnetic dipole) and $^5D_0\rightarrow{}^7F_2$ (electric dipole) transitions of the Eu^{3+} ion, respectively. The intensity of magnetic dipole transition was found to be stronger than that of electric dipole transition. It is suggested that Eu^{3+} had a symmetric environment, which meant that more Eu^{3+} ions occupied Ca^{2+} lattice sites to get an inversion centre and fewer Eu^{3+} ions occupied the grain boundary, surface or defect lattice [15]. When codoped with 7 mol% Li^+ ions, the luminescence intensity of Eu^{3+} at 591 and 612 nm both enhanced by 40%.

The improvement of luminescence was probably due to the substitution of Ca^{2+} sites by Li^+ ions, resulting in disturbance of crystal field environment around the Eu^{3+} ions. The Eu–O bond distortion is expected when Li^+ ions are doped, and the distortion alters the local symmetry of the crystal field around Eu^{3+}. The distortion of the local symmetry around Eu^{3+} increases the transition probabilities which govern various intra-4f shell transitions of the Eu^{3+} ions. Thus, it is possible that the enhancement of luminescence intensity by codoping Li^+ is due to the modified local asymmetry of the crystal field around Eu^{3+} ions [14]. When codoped with 9 mol% Li^+ ions, the luminescence intensity of Eu^{3+} deceased, which was probably due to the formation of defect centres by codoping excess Li^+ [12].

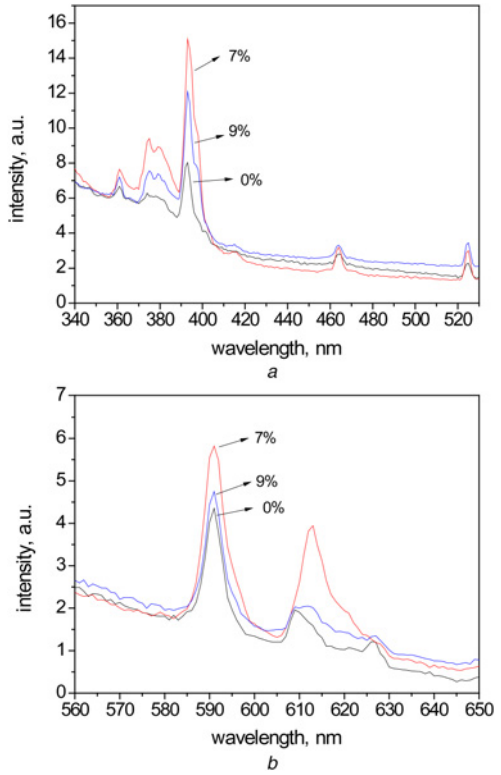

Fig. 4 *Photoluminescence spectra of the samples*
a Excitation spectra (λ_{em} = 591 nm) of CaF_2:Eu^{3+} nanoparticles codoped with 0, 7 and 9 mol% Li^+ ions
b Emission spectra (λ_{ex} = 394 nm) of CaF_2:Eu^{3+} nanoparticles codoped with 0, 7 and 9 mol% Li^+ ions

The time behaviours (λ_{ex} = 394 nm) of the $^5D_0\rightarrow{}^7F_1$ (591 nm) transition for the CaF_2:Eu^{3+} nanoparticles codoped with 0, 7 and 9 mol% Li^+ ions were shown in Fig. 5. All the decay curves of the samples could be well fitted to a double exponential function [15] $I(t) = I_0 + A_1\exp(-t/t_1) + A_2\exp(-t/t_2)$, where I and I_0 are the luminescence intensities at time t and 0. A_1 and A_2 are constant, t is the time, t_1 and t_2 represent the rise and decay times of the transient for the exponential components. The average decay time t_{av} can be calculated by the equation $t_{av} = (A_1t_1^2 + A_2t_2^2)/(A_1t_1 + A_2t_2)$. From the calculation, we get the average times of the $^5D_0$ state of Eu^{3+} ions in the OA capped CaF_2:Eu^{3+} nanoparticles codoped with 0, 7 and 9 mol% Li^+ ions were 5.40, 6.72 and 5.57 ms, respectively. The lifetime increased for 7 mol% Li^+ and reversed for 9 mol% Li^+.

As we know, the experimental lifetime of an excited state, τ, is determined by the theoretical lifetime (τ_{rad}), the non-radiative

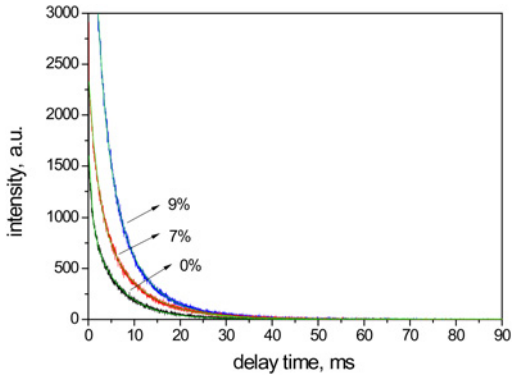

Fig. 5 *Decay profiles of $^5D_0\rightarrow{}^7F_1$ transition (591 nm) of CaF_2:Eu^{3+} nanoparticles codoped with 0, 7 and 9 mol% Li^+ ions (λ_{ex} = 394 nm)*

transition rate (W_{NR}), and the energy transfer rate (W_{ET}), which can be expressed as $1/\tau = 1/\tau_{rad} + W_{NR} + W_{ET}$ [12]. Since there is no energy transfer process in the system, we can attribute the as-observed varying lifetimes (τ) to the tailored local environment of activators (τ_{rad}) and the change of non-radiative decay rate of the excited state (W_{NR}).The lengthening lifetime for 7 mol% Li^+ codoped samples might be ascribed to two reasons. One is the disturbance of crystal field environment around the Eu^{3+} ions, which facilitated the population of the emission state and improved the luminescence of Eu^{3+} ions. The results were fitted with the luminescence properties in steady state conditions (Fig. 4). The other reason is that the codoping of Li^+ increased the distance between Eu^{3+} ions and reduced concentration quenching effect. The decreased lifetime of 9 mol% Li^+ codoped samples was probably due to the increase of the non-radiative transition rate which was caused by the introduction of defect centres.

4. Conclusion: In this study, OA-capped monodisperse CaF_2:Eu^{3+}, Li^+ nanoparticles were synthesised by an eco-friendly solvothermal method. No new crystalline phases are formed after the Li^+ ion incorporation. The main XRD peaks are found to shift to small angles when codoped with 7 mol% Li^+, while the reversed shift direction can be observed for 9 mol% Li^+, indicating that the codoped Li^+ enables the crystal field environment of Eu^{3+} to be changed. The luminescence intensity at 591 and 612 nm is both enhanced by 40% when codoped with 7 mol% Li^+ ions, most likely due to the substitution of Ca^{2+} sites by Li^+ ions, resulting in disturbance of the crystal field environment around the Eu^{3+} ions, leading to the increase of optical dipole transitions.

5. Acknowledgements: This work is supported by the National Natural Science Foundation of China (grant no. 51702051), the Guangdong Natural Science Foundation (grant nos. 2014A030313618 and 2017A030313307) and the Guangdong Education Department Foundation (grant no. 2016KTSCX151) of China.

6 References

[1] Zheng W., Huang P., Tu D., *ET AL.*: 'Lanthanide-doped upconversion nano-bioprobes: electronic structures, optical properties, and biodetection', *Chem. Soc. Rev.*, 2015, **44**, (1), pp. 1379–1415

[2] Zhu Y., Xu W., Cui S., *ET AL.*: 'Controlled size and morphology, and phase transition of YF_3:Yb^{3+},Er^{3+} and YOF:Yb^{3+},Er^{3+} nanocrystals for fine color tuning', *J. Mater. Chem. C*, 2016, **4**, (2), pp. 331–339

[3] Chinen A.B., Guan C.M., Ferrer J.R., *ET AL.*: 'Nanoparticle probes for the detection of cancer biomarkers, cells, and tissues by fluorescence', *Chem. Rev.*, 2015, **115**, (19), pp. 10530–10574

[4] Tou M., Mei Y., Bai S., *ET AL.*: 'Depositing CdS nanoclusters on carbon-modified $NaYF_4$:Yb,Tm upconversion nanocrystals for NIR-light enhanced photocatalysis', *Nanoscale*, 2016, **8**, (1), pp. 553–562

[5] Tao L., Zhou B., Jin W., *ET AL.*: 'Improved multiphoton ultraviolet upconversion photoluminescence in ultrasmall core–shell nanocrystals', *Opt. Lett.*, 2014, **39**, (21), pp. 6265–6268

[6] Ritter B., Krahl T., Rurack K., *ET AL.*: 'Nanoscale CaF_2 doped with Eu^{3+} and Tb^{3+} through fluorolytic sol-gel synthesis', *J. Mater. Chem. C*, 2014, **2**, (40), pp. 8607–8613

[7] Ding M.Y., Ni Y.R., Song Y., *ET AL.*: 'Li^+ ions doping core–shell nanostructures: an approach to significantly enhance upconversion luminescence of lanthanide-doped nanocrystals', *J. Alloys Compd.*, 2015, **623**, (1), pp. 42–48

[8] Singh A.K., Singh S.K., Rai S.B.: 'Role of Li^+ ion in the luminescence enhancement of lanthanide ions: favorable modifications in host matrices', *RSC Adv.*, 2014, **4**, (51), pp. 27039–27061

[9] Wang L., Li X., Li Z., *ET AL.*: 'A new cubic phase for a $NaYF_4$ host matrix offering high upconversion luminescence efficiency', *Adv. Mater.*, 2015, **27**, (37), pp. 5528–5533

[10] Yin W.Y., Tian G., Ren W.L., *ET AL.*: 'Design of multifunctional alkali ion doped CaF_2 upconversion nanoparticles for simultaneous bioimaging and therapy', *Dalton Trans.*, 2014, **43**, (10), pp. 3861–3870

[11] Singh L.P., Srivastava S.K., Mishra R., *ET AL.*: 'Multifunctional hybrid nanomaterials from water dispersible CaF_2:Eu^{3+}, Mn^{2+} and Fe_3O_4 for luminescence and hyperthermia application', *J. Phys. Chem. C.*, 2014, **118**, (31), pp. 18087–18096

[12] Zhao C.Z., Kong X.G., Liu X.M., *ET AL.*: 'Li^+ ion doping: an approach for improving the crystallinity and upconversion emissions of $NaYF_4$:Yb^{3+}, Tm^{3+} nanoparticles', *Nanoscale*, 2013, **5**, (17), pp. 8084–8089

[13] Zhang X.M., Quan Z.W., Yang J., *ET AL.*: 'Solvothermal synthesis of well-dispersed MF_2 (M = Ca, Sr, Ba) nanocrystals and their optical properties', *Nanotechnology*, 2008, **19**, (7), p. 075603 (1–8)

[14] Fan T., Lü J.T.: 'Enhanced 1.5 μm and green upconversion emissions in Y_2O_3:Er^{3+} nanoparticles codoped with Li^+ ions', *Opt. Comm.*, 2013, **300**, (1), pp. 5–7

[15] Sun J.Y., Zhang W.H., Du H.Y., *ET AL.*: 'Hydrothermal synthesis and the enhanced blue upconversion luminescence of $NaYF_4$: nd^{3+}, Tm^{3+}, Yb^{3+}', *Infrared Phys. Technol.*, 2010, **53**, (1), pp. 388–391

doi: 10.1049/mnl.2017.0662